論文 / 著書情報
Article / Book Information

Title	Thermal Properties of the Element and Binary Oxides toward Negative Thermal Expansion: A First-Principles Lattice-Dynamics Study
Authors	Yasuhide Mochizuki, Hiroki Koiso, Kaede Nagamatsu, Soungmin Bae, Toshihiro Isobe, Akira Nakajima
Citation	The Journal of Physical Chemistry C, Vol. 128, Issue 1, pp. 525-535
Pub. date	2024, 1
DOI	https://doi.org/10.1021/acs.jpcc.3c06507
Creative Commons	Information is in the article.

THE JOURNAL OF PHYSICAL CHEMISTRY C
A JOURNAL OF THE AMERICAN CHEMICAL SOCIETY

pubs.acs.org/JPCC
Article

Thermal Properties of the Element and Binary Oxides toward Negative Thermal Expansion: A First-Principles Lattice-Dynamics Study

Yasuhide Mochizuki,* Hiroki Koiso, Kaede Nagamatsu, Soungmin Bae, Toshihiro Isobe, and Akira Nakajima

Cite This: J. Phys. Chem. C 2024, 128, 525−535
Read Online

ACCESS | Metrics & More | Article Recommendations | Supporting Information

ABSTRACT: To establish the design principles of thermal properties of solids, we performed comprehensive calculations of volume thermal expansion coefficients α_V, bulk moduli B_T, average atomic volumes V, and Grüneisen parameters γ in the finite temperature for the 46 elements and 45 binary oxides using first-principles lattice-dynamics calculations. We clarified that (i) a crystal possessing large V tends to have small B_T; (ii) the major role of γ is the determination of the sign of α_V, the value of which is ruled by the crystal structures and coordination numbers; (iii) the transverse-acoustic (TA) and/or low-frequency phonons are responsible for the negative thermal expansion (NTE) behaviors; (iv) the NTE materials prefer the relatively large V with the void space, possessing negative mode-Grüneisen parameters γ_{qv}; and (v) the common feature of the NTE materials is the phonons vibrating forward to the void space. Our study provides a wide perspective on designing low and/or negative thermal expansion materials.

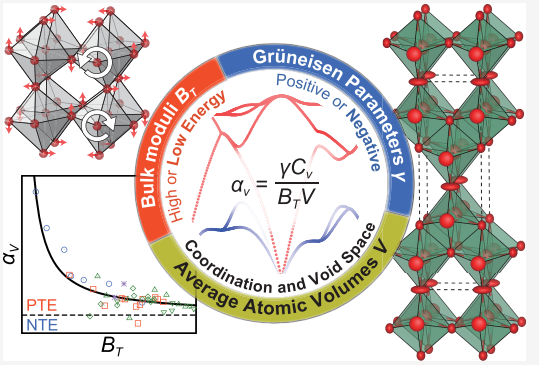

1. INTRODUCTION

Negative thermal expansion (NTE) materials have been vigorously studied for more than a century and are applied to many industrial applications such as heat resistance fillers, microdevices in light-emitting diodes (LED), large-scale integration (LSI), power semiconductors, and micropositioners in the telescopes. The first low thermal expansion (LTE) material (Fe−Ni alloy) and the first NTE material (SiO_2) were reported in 1897[1,2] and 1907,[3,4] respectively. The equation of states for solids was proposed by Mie and Grüneisen in 1903[5] and 1912,[6] respectively, governing the thermal expansion behaviors of harmonic solids. Many representative NTE materials, ZrW_2O_8,[7] ZrV_2O_7,[8] $PbTiO_3$,[9] ScF_3,[10] and $Cd(CN)_2$,[11] have been reported from the mid-20th century to recent 2010. Although a tremendous amount of work on LTE and NTE materials has been dedicated so far,[12−24] a comprehensive study showing the chemical aspects and materials-design concepts for realizing LTE and NTE behaviors is lacking. Specifically, it remains unclear as a nontrivial problem how we design LTE or NTE materials with various combinations of the elements. These fundamental uncertainties stem from unclear correlations between the thermal expansion coefficients and related parameters of crystals.

In this study, we present the systematic calculation results of thermal properties, namely, volume thermal expansion coefficients α_V, bulk moduli B_T, average atomic volumes V, and Grüneisen parameters γ for the 46 unary solids and 45 binary oxides through first-principles lattice-dynamics calculations using quasi-harmonic approximation (QHA). We provide a formulation of α_V based on the Mie−Grüneisen equation of states. From the analytic formulation of α_V, we thoroughly analyze the correlations between α_V, B_T, V, and γ using the calculation results. Some chemical trends of the thermal properties of unary solids and binary oxides are provided and discussed.

2. COMPUTATIONAL DETAILS

The first-principles calculations were carried out using the projector augmented-wave (PAW) method[25] and the PBEsol functional within the generalized gradient approximation[26] as implemented in VASP.[27,28] The cutoff radii and valence electronic configurations of the PAW data sets used in the calculations are given in Table S1 in the Supporting Information. The cutoff energy was set as 550 eV. The phonon dispersions were derived from the calculated force constants using PHONOPY.[29−31] Here, to derive the force constants, we

Received: September 29, 2023
Revised: December 5, 2023
Accepted: December 5, 2023
Published: December 28, 2023

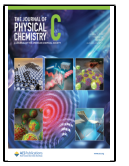

https://doi.org/10.1021/acs.jpcc.3c06507
J. Phys. Chem. C 2024, 128, 525−535

adopted a 2 × 2 × 2 supercell for the cubic, rhombohedral, tetragonal, orthorhombic, and monoclinic structures, while a 3 × 3 × 2 supercell was used for the hexagonal structures. As an exception, we calculated the force constants of Cu_2O ($Pn\bar{3}m$) by expanding the supercell as 4 × 4 × 4 because the negative α_V were largely overestimated in the results from the 2 × 2 × 2 and 3 × 3 × 3 supercells. We did not calculate the thermal properties when a crystal structure has imaginary phonon modes because free energy calculations are unavailable. For the calculations through QHA,[32] we isotropically changed the relaxed lattice constants as −5 to +5% in the unary solids and −0.66 to +0.66% in the binary oxides. Here, in the calculations for the partially occupied 3*d* transition-metal oxides, we used the Dudarev formulation of +*U* correction[33] with the antiferromagnetic configurations to obtain the dynamically stable phases. We applied the +*U* corrections for the on-site 3d electrons in V, Cr, Fe, and Ni as 3, 3, 4, and 7 eV, respectively, the values of which were used in the previous studies.[34−36] The atomic displacement parameters were calculated using PHONOPY.[37,38]

All of the initial crystal structures used in the present study were extracted from Materials Project.[39] The band paths were determined by the seekpath code[40] and from the Brillouin-zone database.[41] The space-group symmetry analyses were performed by SGPLIB[42] as implemented in PHONOPY. Further, the symmetry modes and irreps were analyzed through AMPLIMODES[43,44] and ISODISTORT,[45] respectively.

3. RESULTS AND DISCUSSION

3.1. Thermal Expansion Coefficients of the Elements. We present the calculated and experimentally reported thermal expansion coefficients α_V, bulk moduli B_T, and Grüneisen parameters γ of the elements at 300 K as shown in Figure 1a−c (see Table S2 for the details in the Supporting Information). The calculated and experimental values validate the predictability and accuracy of the QHA employed in this work.

Within the scheme of QHA, the volume thermal expansion coefficient α_V in a solid is given as[12,13,17,52−54]

$$\alpha_V = \frac{\gamma C_V}{B_T V} \tag{1}$$

where γ, C_V, V, and B_T are the Grüneisen parameter, heat capacity at constant volume, volume per one atom (average atomic volume), and bulk moduli, respectively (see Section 3 in the Supporting Information for the detailed derivation of the eq 1). At first, we discuss the correlation between the α_V and B_T based on eq 1 for unary solids as illustrated in Figure 1d. It is shown that the α_V is inversely proportional to the B_T, which is in accordance with eq 1. Here, we present the curves of α_V as a function of B_T by substituting the C_V, γ, and V as $3k_B$, 1, and 25 Å^3 (mean value of average atomic volume for the unary solids), respectively in eq 1. It is apparent that the most crucial factor for determining the thermal expansion coefficients α_V is the bulk moduli B_T: low (high) α_V are owing to high (low) B_T, the chemical trend of which is natural and intuitive. In contrast, it should be denoted that α_V and V are not inversely proportional, as will be discussed in Section 3.2. Moreover, from the calculation results, we found that the higher principal quantum number n of the peripheral electron in *s*- and *p*-block (*d*-block) elements gives rise to lowering (heightening) their bulk moduli. In other words, the *s*- and *p*-block (*d*-block) with a low (high) principal quantum number n possess rigid chemical bonding. This chemical trend would explain the reason why LTE and

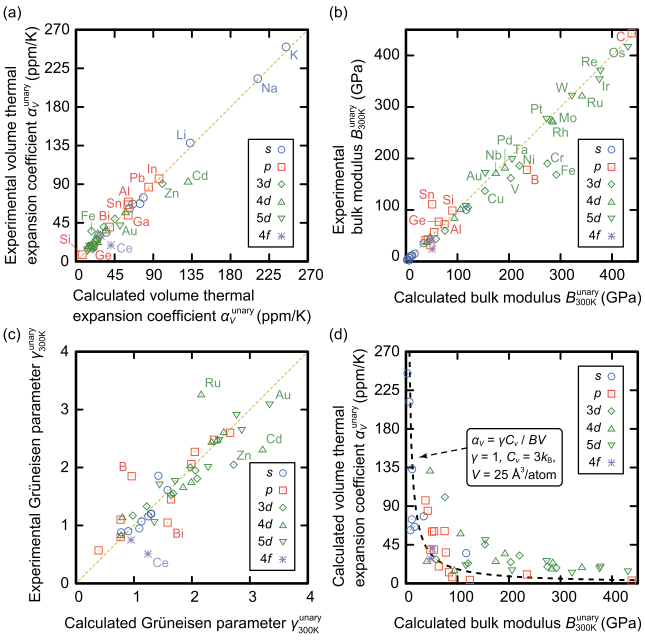

Figure 1. Validations of the calculated (a) volume thermal expansion coefficients α_V, (b) bulk moduli B_T, and (c) Grüneisen parameters γ by using QHA compared to the experimental values. Note that α_V, B_T, and γ are the calculation results in the condition of T = 300 K. Experimental values of α_V, B_T, and γ are referred from refs 46−51. (d) Our calculated volume thermal expansion coefficients as a function of the bulk modulus. The dashed line depicts the relation of α_V and B_T as presented in eq 1 with assuming the C_V, γ, and V as $3k_B$, 1, and 25 Å^3, respectively (see text for the detail).

NTE materials usually include 2*p*-, 3*p*-, 3*d*-, 4*d*- and 5*d*-block elements exhibiting rigid bonding such as ZrW_2O_8,[7,55] ZrV_2O_7,[8] $Y_2Mo_3O_{12}$,[56] $Sc_2W_3O_{12}$,[57] $NbPO_5$,[58] $TaVO_5$,[59] $Zn(CN)_2$,[60] $Cd(CN)_2$,[11] $Cu_2P_2O_7$,[61] $LiAlSiO_4$,[62] $Zr_2SP_2O_{12}$,[63] and $KZr_2(PO_4)_3$.[64,65]

Let us see the chemical trends of calculated bulk moduli B_T, average atomic volumes V, and Grüneisen parameters γ of the elements. The B_T, V, and γ are found to have periodicity (Figure 2a−c). From Figure 2a,b, one can see that the B_T tends to increase as the V decreases. Additionally, as given in Figure 2c, we can also see some chemical trends of the Grüneisen parameters $\gamma_{300\ K}$ as follows: (i) $\gamma_{300\ K}$ of *s*-block elements are not large compared to the other elements; (ii) $\gamma_{300\ K}$ of *p*-block elements tends to increase with larger principal quantum number; and (iii) $\gamma_{300\ K}$ of *d*-block elements increases from left to right in the periodic table. To show the validity of our calculated Grüneisen parameters $\gamma_{300\ K}$, we also compared the previously reported anharmonic parameter η by Rose et al.[66] (Figure 2d). We can also see that our calculated Grüneisen parameters have a positive correlation with the previously reported anharmonic parameters, which reconfirms the validity of our QHA calculations, including the degree of anharmonicity.

3.2. Thermal Properties of Binary Oxides. We also present the calculation results of volume thermal expansion coefficients at 300 K for 45 binary oxides via QHA (Figure 3a, see also Table S3 in the Supporting Information for the numerical data). We note that some binary oxides with imaginary phonon modes were excluded from the analyses due to their ill-defined free energies under QHA. For instance, four typical SiO_2 species are found to have imaginary phonon modes (see Figures S1 and S2 in the Supporting Information).

https://doi.org/10.1021/acs.jpcc.3c06507
J. Phys. Chem. C 2024, 128, 525−535

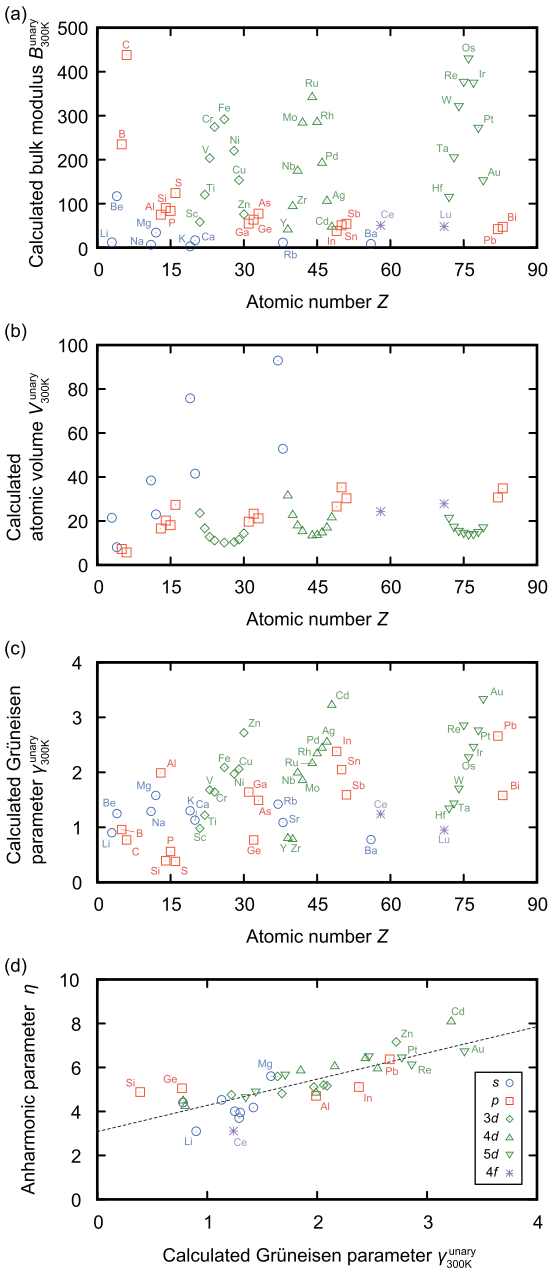

Figure 2. Calculated (a) bulk moduli, (b) atomic volumes, and (c) Grüneisen parameters of the elements with the condition of T= 300 K using quasi-harmonic approximation, which are aligned with the atomic number. (d) Comparison of our calculated Grüneisen parameters of the elements with the previously reported anharmonic parameter η by Rose et al.[66] The black dashed line was derived by least-squares linear fitting.

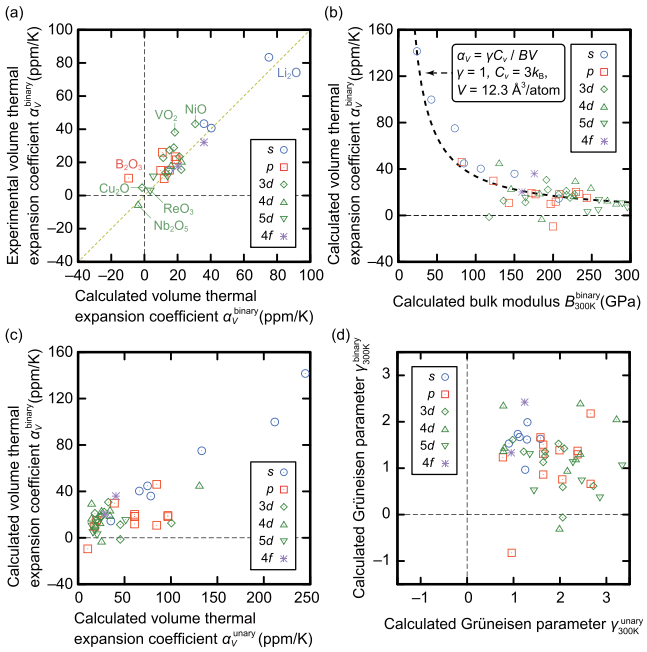

Figure 3. (a) Comparison of experimental and calculated volume thermal expansion coefficients α_V of binary oxides. (b) Calculated volume thermal expansion coefficients as a function of bulk modulus B_T for binary oxides. Experimental thermal expansion coefficients are from refs 67−89. Comparisons of (c) volume thermal expansion coefficients α_V and (d) Grüneisen parameters γ between the elements and binary oxides. α_V, B_T, and γ are the calculation results in the condition of T= 300 K.

The accuracy of calculation results in the binary oxides becomes lower compared to that in the elements for reproducing the experimental results (compare Figures 1a and 3a). Particularly, we observe a large inconsistency of α_V for B_2O_3 between the calculations and experiments, which should be attributed to the phase difference between crystal and amorphous: the experimental α_V of B_2O_3 was measured in glass phase,[67] while our calculated α_V of B_2O_3 was derived from the ideal crystal ($P3_121$ phase).

We then examine the correlation between thermal expansion coefficients α_V and bulk moduli B_T for the binary oxides similar to the unary solids based on eq 1. In Figure 3b, we observe an inverse proportional correlation between α_V and B_T similar to Figure 1d, indicating that eq 1 is also applicable to the binary oxides. This indeed indicates that the most dominant factor in determining α_V is B_T. Originating from this inverse proportional correlation, as discussed further, a larger negative thermal expansion would be obtained in a material exhibiting a negative γ and a smaller B_T.

Figure 3c shows the positive correlation for the thermal expansion coefficients α_V of binary oxides (M_xO_y) and unary counterparts of the element M. On the other hand, the correlation for Grüneisen parameters γ of the elements and binary oxides is less clear (Figure 3d). These results imply that a compound containing an element with large α_V tends to have large thermal expansion coefficients, whereas the degree of anharmonicity in a compound is unrelated to that in the elements. These results indicate the two essential features: (i) the binary oxides composed of the elements with large α_V in their unary solids tend to have large thermal expansion coefficients and (ii) the degree of anharmonicity in the binary oxides is not directly correlated to that of the unary solids. From these results, we conclude that the degree of γ is mainly dependent on crystal structures and coordination environments rather than the the element species. In other words, structural polymorphs with a single chemical composition result in different degrees of anharmonicities and thermal expansion coefficients. We demonstrate this behavior with MgO, CaO, and ZnO of rock-salt (RS) and zincblende (ZB) polymorphs as a case study (Figure 4a,b). While the relatively small α_V values were obtained from the ZB structures compared to those of RS structures (Figure 4a), the B_T values of ZB structures were smaller than those of RS structures (Figure 4b). Intriguingly, the metastable ZB phase of CaO is predicted to exhibit an NTE

https://doi.org/10.1021/acs.jpcc.3c06507
J. Phys. Chem. C 2024, 128, 525−535

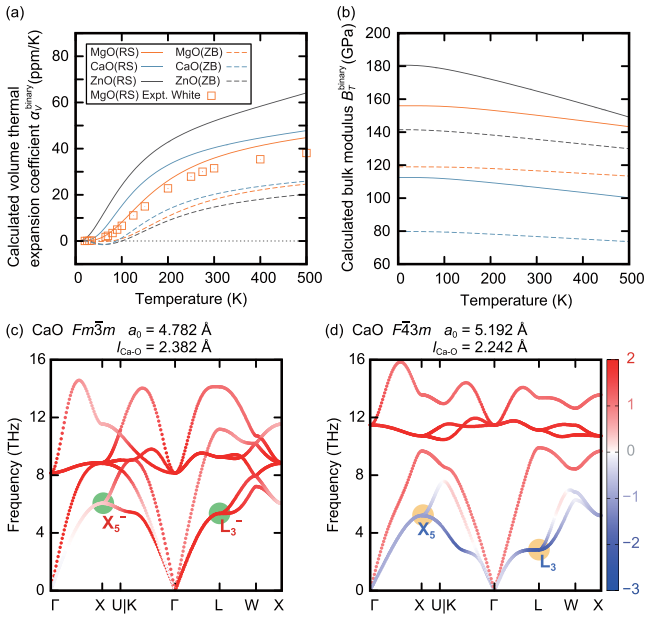

Figure 4. Calculated (a) volume thermal expansion coefficients α_V and (b) bulk moduli B_T for MgO, CaO, and ZnO of rock-salt and zincblende structures as functions of temperature. The experimental values are referred from ref 90. The phonon bands with Grüneisen parameters for CaO of (c) rock-salt and (d) zincblende structures are also shown. The red and blue indicate the positive and negative mode-Grüneisen parameters, respectively. The lattice constants and bond lengths of the RS and ZB structures at 0 K are also indicated.

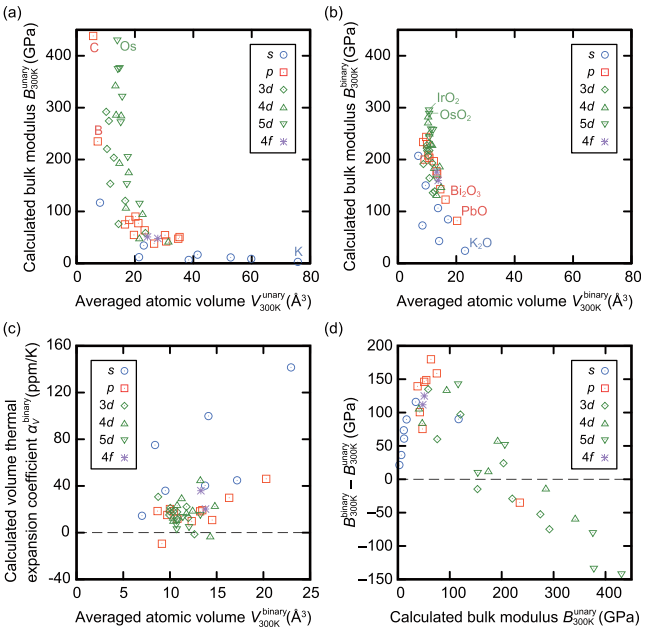

Figure 5. Calculated bulk moduli of (a) the unary systems and (b) binary oxides as a function of average atomic volume. (c) Scatter plot of the volume thermal expansion coefficient of binary oxides and the average atomic volume. (d) Difference of bulk moduli between the elements and the binary oxides as a function of the bulk moduli of the elements.

behavior at low temperatures, while the ground-state RS phase of CaO has large positive thermal expansion (PTE) behavior. The crucial differences in α_V between RS and ZB structures originate from the existence of the negative mode-Grüneisen parameters, which are strongly structure dependent (Figure 4c,d).

We also compared bulk moduli B_T of the unary solids and binary oxides as a function of average atomic volume V (Figure 5a,b). In both systems, B_T has inverse proportional correlations with V and vice versa. As aforementioned in the previous discussion, α_V and B_T have a robust inverse proportional correlation, and hence we can expect a proportional correlation between α_V and V. In fact, a weak proportional correlation can be shown between them (Figure 5c). From eq 1, it may seem to be an inverse proportional correlation between α_V and V; however, actually, they have a weak proportional correlation. In the research field of NTE, it is empirically known that the larger average atomic volume V tends to generate large negative thermal expansion,[91] the reason for which can be explained by the correlation between α_V and V. Let us assume that the Grüneisen parameter γ in eq 1 is negative and α_V is inversely proportional to V as given in eq 1. Then, we get the positive correlation between α_V and V, which contradicts the previous report showing the negative correlation between α_V and V.[91] Considering that B_T and V are dominant for determining α_V, we can catch a glimpse that the major role of Grüneisen parameter in eq 1 is to determine a sign (PTE or NTE). Furthermore, we also show the difference in bulk moduli B_T between the elements and binary oxides (Figure 5d). In the transition metals exhibiting high B_T, such as Cr, Fe, Ni, Cu, Ru, Rh, Re, Os, and Ir, additionally including B, the oxidation of them decreases the B_T, whereas B_T of the other relatively soft metals increases by the oxidation.

3.3. Negative Thermal Expansion Materials among the Elements and Binary Oxides.

From eq 1, as is widely known, the negative α_V (NTE) can be explained only from negative γ because negative values of C_V, B_T, and V cannot be realized. This NTE mechanism is known as the *tension effect*.[17] The role of Grüneisen parameters can also be seen in another aspect of the formula of inner pressure P in crystal. In this case, the static total energy of a crystal E, which is identical to the elastic energy, is given as

$$E(V) = \frac{1}{2} B_T \frac{(V - V_0)^2}{V_0} \tag{2}$$

where V_0 is the average atomic volume in a crystal at 0 K and V is the equilibrium volume per one atom at the finite temperature T. Then, the inner pressure P at finite temperature in a crystal will be given as

$$P + B_T \frac{V - V_0}{V_0} = \frac{1}{V} \sum_{q,\nu} \gamma_{q\nu} U_{q\nu} \tag{3}$$

Assuming that the inner pressure at a finite temperature T is zero with the equilibrium volume V, the volume change $V - V_0$ will be expressed as

$$V - V_0 = \frac{V_0}{BV} \sum_{q,\nu} \gamma_{q\nu} U_{q\nu} \tag{4}$$

On the other hand, in the case of the constant volume ($V = V_0$) at finite temperature, which is a non-equilibrium state, the inner pressure of a crystal will be expressed as

$$P = \frac{1}{V} \sum_{q,\nu} \gamma_{q\nu} U_{q\nu} \tag{5}$$

https://doi.org/10.1021/acs.jpcc.3c06507
J. Phys. Chem. C 2024, 128, 525−535

Both eqs 4 and 5 provide the driving forces of NTE and PTE behaviors. In eq 4, the NTE ($V - V_0 < 0$) is triggered when $\gamma_{q\nu}$ is negative because the phonon internal energy $U_{q\nu}$ is always positive. On the other hand, eq 5 indicates that the driving force of negative (positive) thermal expansion is the phonons with negative (positive) Grüneisen parameters. The phenomena of PTE and NTE in terms of free energy are illustrated in Figure 6a,b. Conclusively, the volume change (NTE and PTE) with

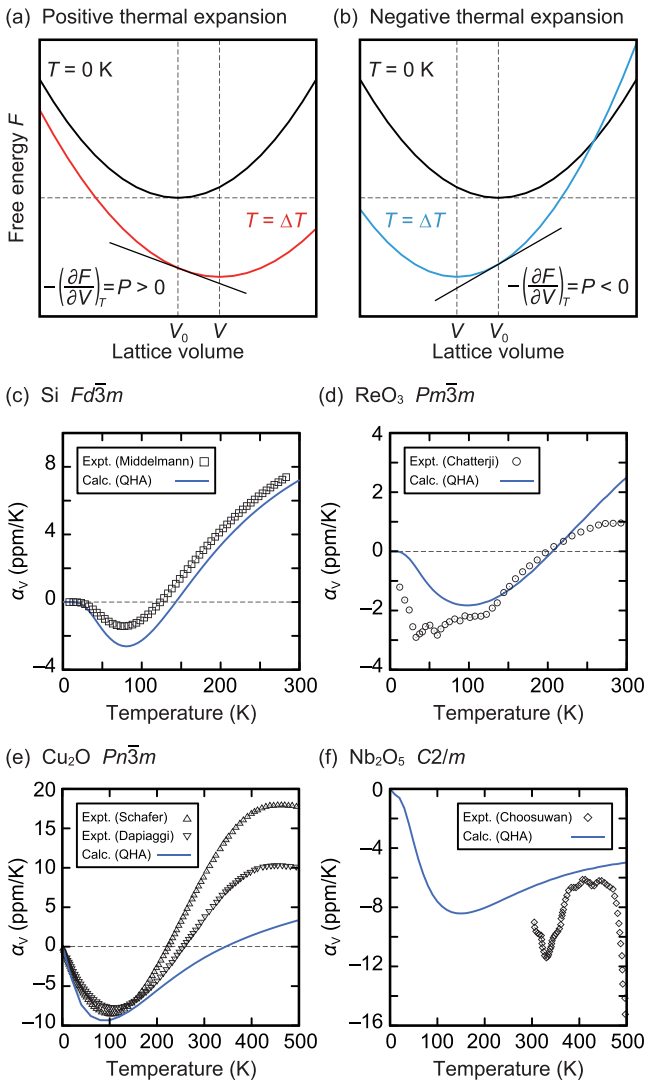

Figure 6. Schematic diagram of Helmholtz free energy as a function of lattice volume in (a) positive and (b) negative thermal-expansion materials. Temperature dependences of calculated thermal expansion coefficients α_V via QHA for (c) Si, (d) ReO_3, (e) Cu_2O, and (f) Nb_2O_5. The experimental α_V were extracted from refs 92−96.

varying temperatures originates from the minimization of free energy, where phonons are extensively involved, whose contribution is determined with the Grüneisen parameter depending on the crystal structure.

We present the calculation results of several NTE materials, Si, ReO_3, Cu_2O, and Nb_2O_5 (Figure 6c−f). The calculation results of these materials via QHA are in good agreement with the experimental results, especially in low temperatures. Some inconsistencies of α_V in high temperatures might be attributed to the anharmonicity, which is not sufficiently captured by QHA (see Section 3 in Supporting Information). QHA considers only the volume dependency of phonon frequencies, while phonon frequencies also depend on the temperature, even with a constant volume. While some limitations of QHA can be overcome with several advanced methods, such as the self-consistent phonon theory,[97] it is still convincible that QHA is one of the most well-balanced methods to capture the nature of thermal expansion with considerably high accuracy and computational cost.[32] The accuracy of QHA was confirmed in the previous computational studies for binary oxides such as Li_2O,[98] w-BeO,[99−101] Na_2O,[102] MgO,[103−106] CaO,[106,107] SrO,[107,108] Al_2O_3,[109,110] Ga_2O_3,[111,112] ZnO,[113] Cu_2O,[114−119] and ReO_3.[93,120,121]

We show phonon bands and mode-Grüneisen parameters of several representative phonon modes of Si, ReO_3, Cu_2O, and Nb_2O_5 in Figure 7a−d. It has been shown that the acoustic phonons play an important role in inducing the NTE behaviors, the phonon modes of which transform like irreducible representations (irreps) X_4 and L_3^- in Si, M_3^+, and R_4^+ in ReO_3, X_4 in Cu_2O, and L_1^-, M_2^-, and A_2^- in Nb_2O_5. Note that all of the aforementioned phonon modes except the M_3^+ mode of ReO_3 are transverse acoustic (TA) phonon modes, while the M_3^+ mode of ReO_3 is a longitudinal acoustic (LA) phonon mode. It has been suggested that the TA phonon modes are responsible for the NTE behavior of ZrW_2O_8,[18,55,122,123] while transverse phonon modes are reported to be crucial for various NTE materials such as ZrV_2O_7, $NbPO_5$, $Cu_2P_2O_7$, Zn_2GeO_4, and $CuScO_2$.[8,58,61,124−126] The reason is that TA phonons ordinally have the lowest frequency among the acoustic branches, leading to large negative Grüneisen parameters. In fact, in 1957, Blackman and Barron suggested that low energy (low frequency) transverse phonons give rise to negative Grüneisen parameters and NTE behaviors.[12,13] Moreover, the TA and/or low-energy phonons with negative Grüneisen parameters should be generally essential for realizing NTE behavior because the phonon lifetime tends to increase with low frequency.[127,128] It is noteworthy that the number of acoustic phonon bands is only 3, whereas that of optical phonon bands is $3N - 3$ (N is the number of atoms in a primitive cell), implying that the acoustic phonons become relatively less important when a unit cell is composed of a large number of atoms. Thus, we consider that the NTE behaviors, the unit cells of which contain a large number of atoms such as ZrW_2O_8 and $Y_2Mo_3O_{12}$, might be attributed to a large number of low-frequency transverse optical (TO) phonons with negative mode Grüneisen parameters, the discussion of which is analogous to that of the previous reports.[17]

Recently, Dove et al. have shown that the NTE behavior of ScF_3 should be explained not only by the phonons at R and M points (rigid unit mode, RUM) but also by the phonons between R and M points (quasi-RUM).[129] Inspired by the previous report,[129] we show the three-dimensional distribution of averaged mode-Grüneisen parameters in half of the first-Brillouin zone for Si, ReO_3, Cu_2O, and Nb_2O_5 as illustrated in Figure 7e−h (see the three-dimensional distribution of averaged mode-Grüneisen parameter for the other oxides in the Supporting Information). We can see through the crucial phonons that contribute to the NTE behavior in Figure 7e−h: the phonons in X and L points contribute to the NTE behavior in Si, while those between R and M points do in ReO_3, which is consistent with the previous report of ScF_3.[129] Additionally, one can see that the phonons around the X (L) point contribute to the NTE behavior in Cu_2O (Nb_2O_5). These results indicate that

https://doi.org/10.1021/acs.jpcc.3c06507
J. Phys. Chem. C 2024, 128, 525−535

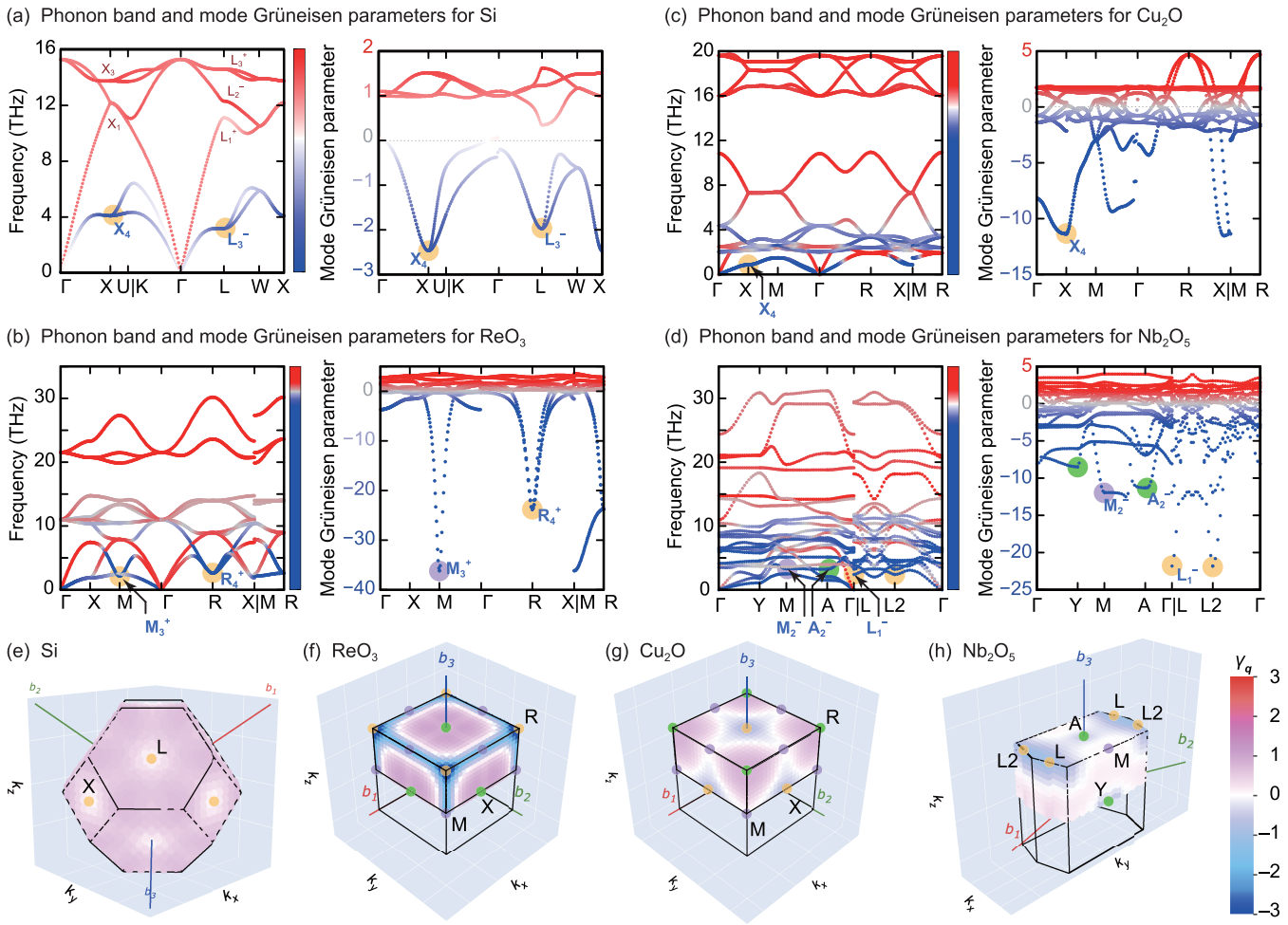

Figure 7. Phonon bands and mode-Grüneisen parameters of (a) Si, (b) ReO_3, (c) Cu_2O, and (d) Nb_2O_5. The red and blue points in the phonon bands indicate the positive and negative mode-Grüneisen parameters, respectively. The three-dimensional distributions of averaged mode-Grüneisen parameters in half of the first Brillouin zone for (e) Si, (f) ReO_3, (g) Cu_2O, and (h) Nb_2O_5 are also illustrated.

not only ScF_3 but also the oxides in Figure 7 have phonon modes, which can be regarded as RUM and quasi-RUM.

We finally present the visualized representative phonon modes of Si, ReO_3, Cu_2O, and Nb_2O_5 with large negative Grüneisen parameters in Figure 8a−d. It is shown that the phonon modes transforming like irreps X_4 and L_3^- of Si, M_3^+ of ReO_3, L_1^-, M_2^-, and A_2^- of Nb_2O_5 are rigid unit modes, while those transforming as irreps R_4^+ of ReO_3 and X_4 of Cu_2O are guitar string modes (see the Supporting Information). Recently, the guitar string effect of ScF_3 was experimentally reported,[130] the structure of which is the same as that of ReO_3. We also present the conventional crystal structures with the calculated atomic displacement parameters at 500 K of the four compounds (Figure 8e), which were visualized by using VESTA.[131] The ellipsoids indicate that the relevant atoms are located in the volume, with a probability of 98%. We can see that the ellipsoidal shapes of Si and those of Cu and O in Cu_2O are close to spherical shapes, indicating that the thermal vibrations in Si and Cu_2O are isotropic. On the other hand, the ellipsoidal shapes of oxygens in ReO_3 and Nb_2O_5 are flat and pancake-shaped, indicating that the thermal vibrations of oxygens in ReO_3 and Nb_2O_5 are anisotropic. The anisotropic thermal vibration might contribute to creating the order of phonons with negative Grüneisen parameters, leading to NTE. Recently, Ritz and Benedek recently suggested that the NTE behavior of $PbTiO_3$ can be attributed to the interplay between phonons and anisotropic elasticity, not to the negative Grüneisen parameters,[132] the discussion of which is still under debate.[133,134] Finally, let us see the isotropic atomic displacement parameters (B parameters) of the relevant compounds. We found that the B parameter is large in the order of Cu_2O, Nb_2O_5, Si, and ReO_3. Note that the large B parameter indicates a drastic thermal vibration. The order of degree of the B parameters should be attributed to the coordination numbers, bond strengths, and atomic masses. For instance, the coordination number of Cu in Cu_2O is 2, while those of Re and Nb in ReO_3 and Nb_2O_5, respectively, are 6. The B parameter of the former is larger than that of the latter.

At last, we compare the NTE behaviors in SiO_2, ReO_3, and metastable ZB CaO. Even in these simple binary oxides, grasping a big picture that unifies the NTE behaviors is challenging. Indeed, the NTE behaviors of SiO_2 (zeolites)[135] and ReO_3 are much different in terms of (i) the existence of pure RUM, which stems from the different number of atoms in their primitive cells, and (ii) the deformation stiffness of SiO_4 tetrahedra and ReO_6 octahedra, as discussed in the previous report.[135] However, considering with another perspective, we can also see the similar characteristics of SiO_2 and ReO_3: both of them have the flexible RUMs that bend the bond angles Si−O−Si and Re−O−Re, stemming from the low-frequency phonon modes, the modes of

https://doi.org/10.1021/acs.jpcc.3c06507
J. Phys. Chem. C 2024, 128, 525−535

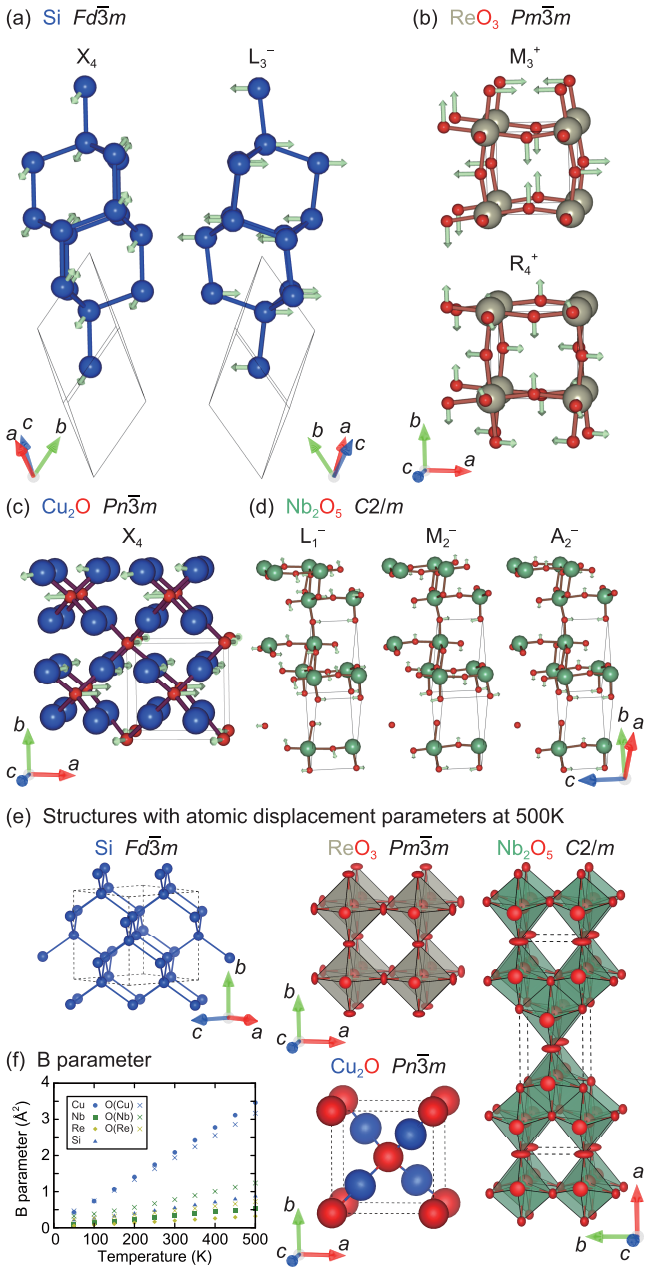

Figure 8. (a−d) Visualized phonon modes transforming like irreps (a) the X_4 and L_3^- of Si, (b) the M_3^+ and R_4^+ of ReO_3, (c) the X_4 of Cu_2O, and (d) the L_1^-, M_2^-, and A_2^- of Nb_2O_5. The black solid lines indicate the relevant primitive unit cells. (e) Conventional crystal structures with calculated atomic displacement parameters at 500 K. (f) Calculated B parameters as a function of temperature.

which are rotational atomic vibrations.[135] Such low-frequency phonon modes that give rotational atomic vibrations do not exist in alkaline earth oxides, such as MgO, CaO, SrO, and BaO, which have RS structures. Interestingly, the metastable ZB CaO and ZnO exhibit the NTE behavior in low temperatures, while the metastable ZB MgO possesses low thermal expansion coefficients compared to RS MgO (Figure 4a). We consider that the low-thermal expansion coefficients of metastable ZB CaO, MgO, and ZnO are attributed to the low-frequency transverse acoustic phonon modes transforming as irreps X_5 and L_3 (Figure 4d), which are analogous to the phonon modes transforming as irreps X_4 and L_3^- in Si (Figure 8a). However, we should be cautious that even the metastable ZB structures do not have low-frequency rotational phonon modes. Thus, the NTE behavior of the ZB structure is far different from those of SiO_2 and ReO_3. Then, what is the common feature that can be observed in all these compounds exhibiting NTE?

Together with all the discussions, we would establish a design concept for achieving phonons with negative mode Grüneisen parameters. The common feature of phonons visualized in Figure 8a−d is that the atomic displacements are toward *void* spaces in the relevant unit cell. Thus, the key factor in realizing NTE would be the existence of void space and relatively small coordination numbers to utilize the transverse phonons, which have small energies for dynamic lattice distortion. This is also the reason why materials with large average atomic volumes and small bulk moduli are usually preferred for NTE materials. This behavior is observed in the case of the RS and ZB structures for CaO (Figure 4), the results of which indicate that the acoustic (optical) phonon modes are softened (hardened) by the coordination-environment modification from relatively dense edge-sharing octahedra (RS structure) into wide corner-sharing tetrahedra (ZB structure).

4. CONCLUSIONS

To establish unified pictures of thermal expansion coefficients and design concepts of negative-thermal expansion (NTE) materials, we performed systematic first-principles lattice-dynamics calculations for the 46 elements and 45 binary oxides via quasi-harmonic approximation (QHA) to examine their thermal properties, that is, thermal expansion coefficients α_V, bulk moduli B_T, average atomic volumes V, and Grüneisen parameters γ. As a result, we have shown that (i) the α_V is determined mainly by the B_T, which has an inverse correlation with α_V; (ii) a crystal possessing large V tends to have small B_T; (iii) the α_V of complex compounds tend to be large (small) when they are composed of the element with large (small) α_V; (iv) the major role of γ, which is ruled by the crystal structures and coordination environment, is the determination of the sign of α_V; (v) the transverse-acoustic (TA) and/or low-frequency phonons are responsible for the negative thermal expansion behaviors; and (vi) the NTE materials prefer the relatively large V, possessing negative mode Grüneisen parameters γ_{qv}. We believe that our results would offer an essential perspective on the development of low- and/or negative thermal expansion materials.

■ ASSOCIATED CONTENT

Supporting Information

The Supporting Information is available free of charge at https://pubs.acs.org/doi/10.1021/acs.jpcc.3c06507.

Derivation of eq 1 and the discussion of anharmonicity; crystal structure schematics of four SiO_2 polymorphs and their phonon bands; calculated and experimentally reported α_V, B_T, and γ at 300 K for the unary solids and binary oxides; cutoff radii and valence electronic configurations of the PAW data sets (PDF)

Visualized phonons with negative mode-Grüneisen parameters for Si, ReO_3, Cu_2O, and Nb_2O_5 (ZIP)

Three-dimensional distribution of averaged mode-Grüneisen parameter for Si and 46 oxides (ZIP)

https://doi.org/10.1021/acs.jpcc.3c06507
J. Phys. Chem. C 2024, 128, 525−535

AUTHOR INFORMATION

Corresponding Author

Yasuhide Mochizuki − *Department of Materials Science and Engineering, School of Materials and Chemical Technology, Tokyo Institute of Technology, Tokyo 152-8550, Japan;* orcid.org/0000-0002-8292-7736; Email: mochizuki.y.af@m.titech.ac.jp

Authors

Hiroki Koiso − *Department of Materials Science and Engineering, School of Materials and Chemical Technology, Tokyo Institute of Technology, Tokyo 152-8550, Japan*

Kaede Nagamatsu − *Department of Materials Science and Engineering, School of Materials and Chemical Technology, Tokyo Institute of Technology, Tokyo 152-8550, Japan*

Soungmin Bae − *Laboratory for Materials and Structures, Institute of Innovative Research, Tokyo Institute of Technology, Yokohama 226-8503, Japan*

Toshihiro Isobe − *Department of Materials Science and Engineering, School of Materials and Chemical Technology, Tokyo Institute of Technology, Tokyo 152-8550, Japan;* orcid.org/0000-0002-2726-6728

Akira Nakajima − *Department of Materials Science and Engineering, School of Materials and Chemical Technology, Tokyo Institute of Technology, Tokyo 152-8550, Japan*

Complete contact information is available at: https://pubs.acs.org/10.1021/acs.jpcc.3c06507

Notes

The authors declare no competing financial interest.

ACKNOWLEDGMENTS

Y.M. was supported by the JSPS KAKENHI grant no. JP22K14471, Nippon Sheet Glass Foundation for Materials Science and Engineering, and Tokyo Tech Challenging Research Award. Further, Y.M. is grateful to Dr. Atsushi Togo for the helpful discussion of quasi-harmonic approximations. Our first-principles calculations were performed by using the computing resources of Research Center for Computational Science at ISSP and Information Technology Center, The University of Tokyo and TSUBAME3.0 supercomputer at Tokyo Institute of Technology. The crystal structures in Figure 8 are visualized with VESTA and TSS Physics webpage.

ABBREVIATIONS

NTE, negative thermal expansion; LTE, low thermal expansion; PTE, positive thermal expansion; QHA, quasi-harmonic approximation; RS, rock-salt; ZB, zincblende; irreps, irreducible representations; TA, transverse acoustic; LA, longitudinal acoustic; TO, transverse optical

REFERENCES

(1) Guillaume, C. Recherches sur les aciers au nickel, Dilata- tions auxtemperatures elevees, resistance electrique. *Acad. Sci.* **1897**, *125*, 235.

(2) Guillaume, C. Invar and its applications. *Nature* **1904**, *71*, 134.

(3) Scheel, K. Versuche ueber die ausdehnung fester koerper, insbesondere von quarz in richtung derhauptachse, platin, palladium und quarzglas bei der temperatur der fluessigen Luft. *Verh. Deutsch. Phys. Ges.* **1907**, *9*, 3.

(4) Scheel, K. Ueber die ausdehnung des quarzglases. *Verh. Deutsch. Phys. Ges.* **1907**, *9*, 719.

(5) Mie, G. Zur kinetischen Theorie der einatomigen Körper. *Annalen der Physik* **1903**, *316*, 657.

(6) Grüneisen, E. Theorie des festen Zustandes einatomiger Elemente. *Annalen der Physik* **1912**, *344*, 257.

(7) Martinek, C.; Hummel, F. Linear Thermal Expansion of Three Tungstates. *J. Am. Ceram. Soc.* **1968**, *51*, 227.

(8) Khosrovani, N.; Sleight, A.; Vogt, T. Structure of ZrV_2O_7 from −263 to 470°C. *J. Solid State Chem.* **1997**, *132*, 355.

(9) Shirane, G.; Hoshino, S. On the Phase Transition in Lead Titanate. *J. Phys. Soc. Jpn.* **1951**, *6*, 265.

(10) Greve, B. K.; Martin, K. L.; Lee, P. L.; Chupas, P. J.; Chapman, K. W.; Wilkinson, A. P. Pronounced Negative Thermal Expansion from a Simple Structure: Cubic ScF_3. *J. Am. Chem. Soc.* **2010**, *132*, 15496.

(11) Phillips, A. E.; Goodwin, A. L.; Halder, G. J.; Southon, P. D.; Kepert, C. J. Nanoporosity and Exceptional Negative Thermal Expansion in Single-Network Cadmium Cyanide. *Angew. Chem., Int. Ed.* **2008**, *47*, 1396.

(12) Blackman, M. On the Thermal Expansion of Solids. *Proc. Phys. Soc. B* **1957**, *70*, 827.

(13) Barron, T. H. K. Grüneisen Parameters for the Equation of State of Solids. *Annals of Physics* **1957**, *1*, 77.

(14) Boysen, H.; Dorner, B.; Frey, F.; Grimm, H. Dynamic structure determination for two interacting modes at the M-point in α- and β-quartz by inelastic neutron scattering. *J. Phys. C: Solid State Phys.* **1980**, *13*, 6127.

(15) Giddy, A. P.; Dove, M. T.; Pawley, G. S.; Heine, V. The Determination of Rigid-Unit Modes as Potential Soft Modes for Displacive Phase Transitions in Framework Crystal Structures. *Acta Cryst. A* **1993**, *49*, 697.

(16) Dove, M. T.; Heine, V.; Hammonds, K. D. Rigid unit modes in framework silicates. *Mineral. Mag.* **1995**, *59*, 629.

(17) Dove, M. T.; Fang, H. Negative thermal expansion and associated anomalous physical properties: review of the lattice dynamics theoretical foundation. *Rep. Prog. Phys.* **2016**, *79*, No. 066503.

(18) Ernst, G.; Broholm, C.; Kowach, G. R.; Ramirez, A. P. Phonon density of states and negative thermal expansion in ZrW_2O_8. *Nature* **1998**, *396*, 147.

(19) Pryde, A. K. A.; Hammonds, K. D.; Dove, M. T.; Heine, V.; Gale, J. D.; Warren, M. C. Rigid unit modes and the negative thermal expansion in ZrW_2O_8. *Phase Transitions* **1997**, *61*, 141.

(20) Miller, W.; Smith, C. W.; Mackenzie, D. S.; Evans, K. E. Negative thermal expansion: a review. *J. Mater. Sci.* **2009**, *44*, 5441.

(21) Takenaka, K. Negative thermal expansion materials: technological key for control of thermal expansion. *Sci. Technol. Adv. Mater.* **2012**, *13*, No. 013001.

(22) Chen, J.; Hu, L.; Deng, J.; Xing, X. Negative thermal expansion in functional materials: controllable thermal expansion by chemical modifications. *Chem. Soc. Rev.* **2015**, *44*, 3522.

(23) Romao, C. P.; Perras, F. A.; Werner-Zwanziger, U.; Lussier, J. A.; Miller, K. A.; Calahoo, C.; Zwanziger, J. W.; Bieringer, M.; Marinkovic, B. A.; Bryce, D. L.; et al. Zero Thermal Expansion in $ZrMgMo_3O_{12}$: NMR Crystallography Reveals Origins of Thermoelastic Properties. *Chem. Mater.* **2015**, *27*, 2633.

(24) Ducamp, M.; Coudert, F. Systematic Study of the Thermal Properties of Zeolitic Frameworks. *J. Phys. Chem. C* **2021**, *125*, 15647.

(25) Blöchl, P. E. Projector augmented-wave method. *Phys. Rev. B* **1994**, *50*, 17953.

(26) Perdew, J. P.; Ruzsinszky, A.; Csonka, G. I.; Vydrov, O. A.; Scuseria, G. E.; Constantin, L. A.; Zhou, X.; Burke, K. Restoring the Density-Gradient Expansion for Exchange in Solids and Surfaces. *Phys. Rev. Lett.* **2008**, *100*, No. 136406.

(27) Kresse, G.; Furthmüller, J. Efficient iterative schemes for *ab initio* total-energy calculations using a plane-wave basis set. *Phys. Rev. B* **1996**, *54*, 11169.

(28) Kresse, G.; Joubert, D. From ultrasoft pseudopotentials to the projector augmented-wave method. *Phys. Rev. B* **1999**, *59*, 1758.

(29) Togo, A.; Tanaka, I. First-principles phonon calculations in materials science. *Scr. Mater.* **2015**, *108*, 1.

(30) Togo, A.; Chaput, L.; Tadano, T.; Tanaka, I. Implementation strategies in phonopy and phono3py. *J. Phys.: Condens. Matter* **2023**, *35*, No. 353001.
(31) Togo, A. First-principles Phonon Calculations with Phonopy and Phono3py. *J. Phys. Soc. Jpn.* **2023**, *92*, No. 012001.
(32) Togo, A.; Chaput, L.; Tanaka, I.; Hug, G. First-principles phonon calculations of thermal expansion in Ti_3SiC_2, Ti_3AlC_2, and Ti_3GeC_2. *Phys. Rev. B* **2010**, *81*, No. 174301.
(33) Dudarev, S. L.; Botton, G. A.; Savrasov, S. Y.; Humphreys, C. J.; Sutton, A. P. Electron-energy-loss spectra and the structural stability of nickel oxide: An LSDA+U study. *Phys. Rev. B* **1998**, *57*, 1505.
(34) Takahashi, A.; Kumagai, Y.; Miyamoto, J.; Mochizuki, Y.; Oba, F. Machine learning models for predicting the dielectric constants of oxides based on high-throughput first-principles calculations. *Phys. Rev. Mater.* **2020**, *4*, No. 103801.
(35) Mochizuki, Y.; Akamatsu, H.; Kumagai, Y.; Oba, F. Strain-engineered Peierls instability in layered perovskite $La_3Ni_2O_7$ from first principles. *Phys. Rev. Mater.* **2018**, *2*, No. 125001.
(36) Jain, A.; Hautier, G.; Ong, S. P.; Moore, C. J.; Fischer, C. C.; Persson, K. A.; Ceder, G. Formation enthalpies by mixing GGA and GGA + *U* calculations. *Phys. Rev. B* **2011**, *84*, No. 045115.
(37) Lane, N. J.; Vogel, S. C.; Hug, G.; Togo, A.; Chaput, L.; Hultman, L.; Barsoum, M. W. Neutron diffraction measurements and first-principles study of thermal motion of atoms in select $M_{n+1}AX_n$ and binary *MX* transition-metal carbide phases. *Phys. Rev. B* **2012**, *86*, No. 214301.
(38) Deringer, V. L.; Stoffel, R. P.; Togo, A.; Eck, B.; Meven, M.; Dronskowski, R. *Ab initio* ORTEP drawings: a case study of N-based molecular crystals with different chemical nature. *CrystEngComm* **2014**, *16*, 10907.
(39) Jain, A.; Ong, S. P.; Hautier, G.; Chen, W.; Richards, W. D.; Dacek, S.; Cholia, S.; Gunter, D.; Skinner, D.; Ceder, G.; et al. Commentary: The Materials Project: A materials genome approach to accelerating materials innovation. *APL Mater.* **2013**, *1*, No. 011002.
(40) Hinuma, Y.; Pizzi, G.; Kumagai, Y.; Oba, F.; Tanaka, I. Band structure diagram paths based on crystallography. *Comput. Mater. Sci.* **2017**, *128*, 140.
(41) Aroyo, M. I.; Orobengoa, D.; de la Flor, G.; Tasci, E. S.; Perez-Mato, J. M.; Wondratschek, H. Brillouin-zone database on the Bilbao Crystallographic Server. *Acta Crystallogr., Sect. A: Found. Adv.* **2014**, *70*, 126.
(42) Togo, A.; Tanaka, I.et al.arXiv **2018**, 1808.01590 https://arxiv.org/abs/1808.01590. (accessed 2023−06−10).
(43) Orobengoa, D.; Capillas, C.; Aroyo, M. I.; Perez-Mato, J. M. AMPLIMODES: symmetry-mode analysis on the Bilbao Crystallographic Server. *J. Appl. Crystallogr.* **2009**, *42*, 820.
(44) Perez-Mato, J. M.; Orobengoa, D.; Aroyo, M. I. Mode Crystallography of distorted structures. *Acta Cryst. A* **2010**, *66*, 558.
(45) Campbell, B. J.; Stokes, H. T.; Tanner, D. E.; Hatch, D. M. ISODISPLACE: An Internet Tool for Exploring Structural Distortions. *J. Appl. Crystallogr.* **2006**, *39*, 607.
(46) Lide, D. R. *CRC Handbook of Chemistry and Physics*; CRC Press: Boca Raton, FL, 2005.
(47) Aschcroft, N. W.; Mermin, N. D. *Solid State Physics*; Saunders College: New York, 1976.
(48) Gschneidner, K. A. Physical Properties and Interrelationships of Metallic and Semimetallic Elements. *Solid State Physics* **1964**, *16*, 275.
(49) Hasegawa, M.; Young, W. Gruneisen parameters for simple metals. *J. Phys. F: Met. Phys.* **1980**, *10*, 225.
(50) Gilvarry, J. Grüneisen's Constant for Some Metals. *J. Chem. Phys.* **1955**, *23*, 1925.
(51) Kittel, C. *Introduction to Solid State Physics*; John Wiley & Sons: New York, 2005.
(52) Born, M.; Huang, K. *Dynamical Theory of Crystal Lattices*; Oxford University Press: New York, 1954.
(53) Sharma, P. K.; Singh, N. Gruneisen Parameter of Cubic Metals. *Phys. Rev. B* **1970**, *1*, 4635.
(54) Shen, Y.; Saunders, C.; Bernal, C.; Abernathy, D. L.; Manley, M. E.; Fultz, B. Anharmonic Origin of the Giant Thermal Expansion of NaBr. *Phys. Rev. Lett.* **2020**, *125*, No. 085504.
(55) Mary, T. A.; Evans, J. S. O.; Vogt, T.; Sleight, A. W. Negative Thermal Expansion from 0.3 to 1050 K in ZrW_2O_8. *Science* **1996**, *272*, 90.
(56) Marinkovic, B. A.; Ari, M.; de Avillez, R. R.; Rizzo, F.; Ferreira, F. F.; Miller, K. J.; Johnson, M. B.; White, M. A. Correlation between AO_6 Polyhedral Distortion and Negative Thermal Expansion in Orthorhombic $Y_2Mo_3O_{12}$ and Related Materials. *Chem. Mater.* **2009**, *21*, 2886.
(57) Evans, J. S. O.; Mary, T. A.; Sleight, A. W. Negative Thermal Expansion in $Sc_2(WO_4)_3$. *J. Solid State Chem.* **1998**, *137*, 148.
(58) Amos, T.; Sleight, A. W. Negative Thermal Expansion in Orthorhombic $NbOPO_4$. *J. Solid State Chem.* **2001**, *160*, 230.
(59) Wang, X.; Huang, Q.; Deng, J.; Yu, R.; Chen, J.; Xing, X. Phase Transformation and Negative Thermal Expansion in $TaVO_5$. *Inorg. Chem.* **2011**, *50*, 2685.
(60) Chapman, K. W.; Chupas, P. J. Pressure Enhancement of Negative Thermal Expansion Behavior and Induced Framework Softening in Zinc Cyanide. *J. Am. Chem. Soc.* **2007**, *129*, 10090.
(61) Shi, N.; Sanson, A.; Gao, Q.; Sun, Q.; Ren, Y.; Huang, Q.; de Souza, D. O.; Xing, X.; Chen, J. Strong Negative Thermal Expansion in a Low-Cost and Facile Oxide of $Cu_2P_2O_7$. *J. Am. Chem. Soc.* **2020**, *142*, 3088.
(62) Gillery, F. H.; Bush, E. A. Thermal Contraction of β-Eucryptite-. ($Li_2O.Al_2O_3.2SiO_2$) by X-Ray and Dilatometer Methods. *J. Am. Ceram. Soc.* **1959**, *42*, 175.
(63) Isobe, T.; Hayakawa, Y.; Adachi, Y.; Uehara, R.; Matsushita, S.; Nakajima, A. Negative thermal expansion in α-$Zr_2SP_2O_{12}$ based on phase transition- and framework-type mechanisms. *NPG Asia Mater.* **2020**, *12*, 80.
(64) Oota, T.; Wamai, I. Thermal Expansion Behavior of $NaZr_2(PO_4)_3$ Type Compounds. *J. Am. Ceram. Soc.* **1986**, *69*, 1.
(65) Miyazaki, H.; Ushiroda, I.; Itomura, D.; Hirashita, T.; Adachi, N.; Ota, T. Thermal Expansion of $NaZr_2(PO_4)_3$ Family Ceramics in a Low-Temperature Range. *Jpn. J. Appl. Phys.* **2008**, *47*, 7262.
(66) Rose, J. H.; Smith, J. R.; Guinea, F.; Ferrante, J. Universal features of the equation of state of metals. *Phys. Rev. B* **1984**, *29*, 2963.
(67) Alderman, O. L. G.; Ferlat, G.; Baroni, A.; Salanne, M.; Micoulaut, M.; Benmore, C. J.; Lin, A.; Tamalonis, A.; Weber, J. K. R. Liquid B_2O_3 up to 1700 K: x-ray diffraction and boroxol ring dissolution. *J. Phys.: Condens. Matter* **2015**, *27*, No. 455104.
(68) Hull, S.; Farley, T. W. D.; Hayes, W.; Hutchings, M. T. The elastic properties of lithium oxide and their variation with temperature. *J. Nucl. Mater.* **1988**, *160*, 125.
(69) Kozlovskii, Y. M.; Stankus, S. V. Thermal expansion of beryllium oxide in the temperature interval 20−1550°C. *High Temperature* **2014**, *52*, 536.
(70) De Almeida, M.; Brook, R. J.; Carruthers, T. G. Thermal expansion of ceramics in the MgO-CaO system. *J. Mater. Sci.* **1979**, *14*, 2191.
(71) Cazzato, A.; Faber, K. T. Fracture Energy of GlassAlumina Interfaces via the Bimaterial Bend Test. *J. Am. Ceram. Soc.* **1997**, *80*, 181.
(72) Stecura, S.; Campbell, W. J. *Thermal expansion and phase inversion of rare-earth oxides*. United States, 1960. https://www.osti.gov/biblio/4840970. DOI:10.2172/4840970 (accessed 2023−06−10)
(73) Sugiyama, K.; Takeuchi, Y. The crystal structure of rutile as a function of temperature up to 1600°C. *Zeitschrift fur Kristallographie* **1991**, *194*, 305.
(74) Rimshow, S. J.; Ketchen, E. E. *Strontium-90 data sheets*; Oak Bridge National Laboratory, ORNL-4188, 1967. (accessed 2023−06−10).
(75) Eckert, L. J.; Bradt, R. C. Thermal expansion of corundum structure Ti_2O_3 and V_2O_3. *J. Appl. Phys.* **1973**, *44*, 3470.
(76) Krishna Rao, K. V.; Nagender Naidu, S. V.; Iyengar, L. Thermal Expansion of Tetragonal Phase of VO_2. *J. Phys. Soc. Jpn.* **1967**, *23*, 1380.

(77) Pai, R. V.; Krishnan, K.; Dash, S.; Mukerjee, S. K.; Venugopal, V. Synthesis, characterization and thermal expansion of $Cr_{2-x}Ti_xO_{3+\delta}$. *J. Alloys Compd.* **2010**, *507*, 267.
(78) Becker, R.; Hartwig, H.; Köppe, H.; Vanecek, H.; Velić, P.; Warncke, R.; Zelle, A. *Gmelin Handbuch der Anorganischen Chemie*; Springer, 1978; page 77.
(79) Corbel, G.; Lacorre, P. Compatibility evaluation between $La_2Mo_2O_9$ fast oxide-ion conductor and Ni-based materials. *J. Solid State Chem.* **2006**, *179*, 1339.
(80) Tiano, W.; Dapiaggi, M.; Artioli, G. Thermal expansion in cuprite-type structures from 10 K to decomposition temperature: Cu_2O and Ag_2O. *J. Appl. Crystallogr.* **2003**, *36*, 1461.
(81) Tröger, L.; Yokoyama, T.; Arvanitis, D.; Lederer, T.; Tischer, M.; Baberschke, K. Determination of bond lengths, atomic mean-square relative displacements, and local thermal expansion by means of soft-x-ray photoabsorption. *Phys. Rev. B* **1994**, *49*, 888.
(82) Víllora, E. G.; Shimamura, K.; Ujiie, T.; Aoki, K. Electrical conductivity and lattice expansion of β-Ga_2O_3 below room temperature. *Appl. Phys. Lett.* **2008**, *92*, No. 202118.
(83) Suzuki, S.; Takahashi, M.; Hikich, Y. Free Volume of Network-Forming Oxide Glasses in the Systems P_2O_5-(GeO_2,TeO_2,Sb_2O_3,V_2O_5). *J. Am. Ceram. Soc.* **1987**, *70*, C213.
(84) Haggerty, R. P.; Sarin, P.; Apostolov, Z. D.; Driemeyer, P. E.; Kriven, W. M. Thermal Expansion of HfO_2 and ZrO_2. *J. Am. Ceram. Soc.* **2014**, *97*, 2213.
(85) Manning, W. R.; Hunter, O.; Calderwood, F. W.; Stacy, D. W. Thermal Expansion of Nb_2O_5. *J. Am. Ceram. Soc.* **1972**, *55*, 342.
(86) Kundra, K. D.; Ali, S. Z. Thermal expansion of In_2O_3. *J. Appl. Crystallogr.* **1970**, *3*, 543.
(87) Zhu, H.; Li, Q.; Yang, C.; Zhang, Q.; Ren, Y.; Gao, Q.; Wang, N.; Lin, K.; Deng, J.; Chen, J.; et al. Twin Crystal Induced near Zero Thermal Expansion in SnO_2 Nanowires. *J. Am. Chem. Soc.* **2018**, *140*, 7403.
(88) Wu, S.; Chan, H. M.; Harmer, M. P. Compositional tailoring of the thermal expansion coefficient of tantalum (V) oxide. *J. Mater. Sci.* **2006**, *41*, 689.
(89) Chang, T.-S.; Trucano, P. Lattice parameter and thermal expansion of ReO_3 between 291 and 464 K. *J. Appl. Crystallogr.* **1978**, *11*, 286.
(90) White, G. K.; Anderson, O. L. Grüneisen Parameter of Magnesium Oxide. *J. Appl. Phys.* **1966**, *37*, 430.
(91) Gao, Q.; Wang, J.; Sanson, A.; Sun, Q.; Liang, E.; Xing, X.; Chen, J. Discovering Large Isotropic Negative Thermal Expansion in Framework Compound $AgB(CN)_4$ via the Concept of Average Atomic Volume. *J. Am. Chem. Soc.* **2020**, *142*, 6935.
(92) Middelmann, T.; Walkov, A.; Bartl, G.; Schödel, R. Thermal expansion coefficient of single-crystal silicon from 7 to 293 K. *Phys. Rev. B* **2015**, *92*, No. 174113.
(93) Chatterji, T.; Henry, P. F.; Mittal, R.; Chaplot, S. L. Negative thermal expansion of ReO_3: Neutron diffraction experiments and dynamical lattice calculations. *Phys. Rev. B* **2008**, *78*, No. 134105.
(94) Schäfer, W.; Kirfel, A. Neutron powder diffraction study of the thermal expansion of cuprite. *Appl. Phys. A: Mater. Sci. Process.* **2002**, *74*, s1010.
(95) Dapiaggi, M.; Tiano, W.; Artioli, G.; Sanson, A.; Fornasini, P. The thermal behaviour of cuprite: An XRD−EXAFS combined approach. *Nucl. Instrum. Methods Phys. Res., Sect. B* **2003**, *200*, 231.
(96) Choosuwan, H.; Guo, R.; Bhalla, A. S.; Balachandran, U. Negative thermal expansion behavior in single crystal and ceramic of Nb_2O_5-based compositions. *J. Appl. Phys.* **2002**, *91*, 5051.
(97) Oba, Y.; Tadano, T.; Akashi, R.; Tsuneyuki, S. First-principles study of phonon anharmonicity and negative thermal expansion in ScF_3. *Phys. Rev. Mater.* **2019**, *3*, No. 033601.
(98) Goel, P.; Choudhury, N.; Chaplot, S. L. Superionic behavior of lithium oxide Li_2O: A lattice dynamics and molecular dynamics study. *Phys. Rev. B* **2004**, *70*, No. 174307.
(99) Wdowik, U. D. Structural stability and thermal properties of BeO from the quasiharmonic approximation. *J. Phys.: Condens. Matter* **2010**, *22*, No. 045404.
(100) Luo, F.; Cheng, Y.; Cai, L.-C.; Chen, X.-R. Structure and thermodynamic properties of BeO: Empirical corrections in the quasiharmonic approximation. *J. Appl. Phys.* **2013**, *113*, No. 033517.
(101) Malakkal, L.; Szpunar, B.; Siripurapu, R. K.; Zuniga, J. C.; Szpunar, J. A. Thermal conductivity of wurtzite and zinc blende cubic phases of BeO from *ab initio* calculations. *Solid State Sci.* **2017**, *65*, 79.
(102) Zhuravlev, Y. N.; Korabel'nikov, D. V.; Aleinikova, M. V. *Ab initio* calculations of the thermodynamic parameters of lithium, sodium, and potassium oxides under pressure. *Phys. Solid State* **2012**, *54*, 1518.
(103) Hemley, R. J.; Jackson, M. D.; Gordon, R. G. First-principles theory for the equations of state of minerals at high pressures and temperatures: Application to MgO. *Geophys. Res. Lett.* **1985**, *12*, 247.
(104) Isaak, D. G.; Cohen, R. E.; Mehl, M. J. Calculated elastic and thermal properties of MGO at high pressures and temperatures. *J. Geophys. Res.: Solid Earth* **1990**, *95*, 7055.
(105) Karki, B. B.; Wentzcovitch, R. M.; de Gironcoli, S.; Baroni, S. High-pressure lattice dynamics and thermoelasticity of MgO. *Phys. Rev. B* **2000**, *61*, 8793.
(106) Erba, A.; Shahrokhi, M.; Moradian, R.; Dovesi, R. On how differently the quasi-harmonic approximation works for two isostructural crystals: Thermal properties of periclase and lime. *J. Chem. Phys.* **2015**, *142*, No. 044114.
(107) Ruppin, R. Grüneisen parameters and thermal expansion of CaO and SrO. *Solid State Commun.* **1972**, *10*, 1053.
(108) Souadkia, M.; Bennecer, B.; Kalarasse, F. *Ab initio* lattice dynamics and thermodynamic properties of SrO under pressure. *J. Phys. Chem. Solids* **2012**, *73*, 129.
(109) Shang, S.-L.; Zhang, H.; Wang, Y.; Liu, Z.-K. Temperature-dependent elastic stiffness constants of α- and θ-Al_2O_3 from first-principles calculations. *J. Phys.: Condens. Matter* **2010**, *22*, No. 375403.
(110) Huang, L.-F.; Lu, X.-Z.; Tennessen, E.; Rondinelli, J. M. An efficient *ab-initio* quasiharmonic approach for the thermodynamics of solids. *Comput. Mater. Sci.* **2016**, *120*, 84.
(111) Yoshioka, S.; Hayashi, H.; Kuwabara, A.; Oba, F.; Matsunaga, K.; Tanaka, I. Structures and energetics of Ga_2O_3 polymorphs. *J. Phys.: Condens. Matter* **2007**, *19*, No. 346211.
(112) Santia, M. D.; Tandon, N.; Albrecht, J. D. Thermal Properties of β-Ga_2O_3 from First Principles. *MRS Adv.* **2016**, *1*, 109.
(113) Wang, Z.; Wang, F.; Wang, L.; Jia, Y.; Sun, Q. First-principles study of negative thermal expansion in zinc oxide. *J. Appl. Phys.* **2013**, *114*, No. 063508.
(114) Mittal, R.; Chaplot, S. L.; Mishra, S. K.; Bose, P. P. Inelastic neutron scattering and lattice dynamical calculation of negative thermal expansion compounds Cu_2O and Ag_2O. *Phys. Rev. B* **2007**, *75*, No. 174303.
(115) Bohnen, K.-P.; Heid, R.; Pintschovius, L.; Soon, A.; Stampfl, C. *Ab initio* lattice dynamics and thermal expansion of Cu_2O. *Phys. Rev. B* **2009**, *80*, No. 134304.
(116) Rimmer, L. H. N.; Dove, M. T.; Winkler, B.; Wilson, D. J.; Refson, K.; Goodwin, A. L. Framework flexibility and the negative thermal expansion mechanism of copper(I) oxide Cu_2O. *Phys. Rev. B* **2014**, *89*, No. 214115.
(117) Gupta, M. K.; Mittal, R.; Chaplot, S. L.; Rols, S. Phonons, nature of bonding, and their relation to anomalous thermal expansion behavior of M_2O (M = Au, Ag, Cu). *J. Appl. Phys.* **2014**, *115*, No. 093507.
(118) Linnera, J.; Erba, A.; Karttunen, A. J. Negative thermal expansion of Cu_2O studied by quasi-harmonic approximation and cubic force-constant method. *J. Chem. Phys.* **2019**, *151*, No. 184109.
(119) Saunders, C. N.; Kim, D. S.; Hellman, O.; Smith, H. L.; Weadock, N. J.; Omelchenko, S. T.; Granroth, G. E.; Bernal-Choban, C. M.; Lohaus, S. H.; et al. Thermal expansion and phonon anharmonicity of cuprite studied by inelastic neutron scattering and ab initio calculations. *Phys. Rev. B* **2022**, *105*, No. 174308.
(120) Wdowik, U. D.; Parlinski, K.; Chatterji, T.; Rols, S.; Schober, H. Lattice dynamics of rhenium trioxide from the quasiharmonic approximation. *Phys. Rev. B* **2010**, *82*, No. 104301.
(121) Liu, Y.; Wang, Z.; Wu, M.; Sun, Q.; Chao, M.; Jia, Y. Negative thermal expansion in isostructural cubic ReO_3 and ScF_3: A comparative study. *Comput. Mater. Sci.* **2015**, *107*, 157.

https://doi.org/10.1021/acs.jpcc.3c06507
J. Phys. Chem. C 2024, 128, 525−535

(122) Evans, J. S. O.; Mary, T. A.; Vogt, T.; Subramanian, M. A.; Sleight, A. W. Negative thermal expansion in ZrW_2O_8 and HfW_2O_8. *Chem. Mater.* **1996**, *8*, 2809.
(123) Pryde, A.; Hammonds, K. D.; Dove, M. T.; Heine, V.; Gale, J. D.; Warren, M. C. Origin of the negative thermal expansion in ZrW_2O_8 and ZrV_2O_7. *J. Phys.: Condens. Matter* **1996**, *8*, 10973.
(124) Yuan, H.; Gao, Q.; Xu, P.; Guo, J.; He, L.; Sanson, A.; Chao, M.; Liang, E. Understanding Negative Thermal Expansion of Zn_2GeO_4 through Local Structure and Vibrational Dynamics. *Inorg. Chem.* **2021**, *60*, 1499.
(125) Li, J.; Yokochi, A.; Amos, T. G.; Sleight, A. W. Strong Negative Thermal Expansion along the O−Cu−O Linkage in $CuScO_2$. *Chem. Mater.* **2002**, *14*, 2602.
(126) Shi, N.; Sanson, A.; Sun, Q.; Fan, L.; Venier, A.; Oliveira de Souza, D.; Xing, X.; Chen, J. Strong Negative Thermal Expansion of Cu_2PVO_7 in a Wide Temperature Range. *Chem. Mater.* **2021**, *33*, 1321.
(127) Togo, A.; Chaput, L.; Tanaka, I. Distributions of phonon lifetimes in Brillouin zones. *Phys. Rev. B* **2015**, *91*, No. 094306.
(128) Tadano, T.; Tsuneyuki, S. Self-consistent phonon calculations of lattice dynamical properties in cubic $SrTiO_3$ with first-principles anharmonic force constants. *Phys. Rev. B* **2015**, *92*, No. 054301.
(129) Dove, M. T.; Wei, Z.; Phillips, A. E.; Keen, D. A.; Refson, K. Which phonons contribute most to negative thermal expansion in ScF_3? *APL Mater.* **2023**, *11*, No. 041130.
(130) Hu, L.; Chen, J.; Sanson, A.; Wu, H.; Guglieri Rodriguez, C.; Olivi, L.; Ren, Y.; Fan, L.; Deng, J.; Xing, X. New Insights into the Negative Thermal Expansion: Direct Experimental Evidence for the "Guitar-String" Effect in Cubic ScF_3. *J. Am. Chem. Soc.* **2016**, *138*, 8320.
(131) Momma, K.; Izumi, F. VESTA 3 for three-dimensional visualization of crystal. *J. Appl. Crystallogr.* **2011**, *44*, 1272.
(132) Ritz, E. T.; Benedek, N. A. Interplay between Phonons and Anisotropic Elasticity Drives Negative Thermal Expansion in $PbTiO_3$. *Phys. Rev. Lett.* **2018**, *121*, No. 255901.
(133) Mittal, R.; Gupta, M. K.; Singh, B.; Chaplot, S. L. Comment on Interplay between Phonons and Anisotropic Elasticity Drives Negative Thermal Expansion in $PbTiO_3$. *Phys. Rev. Lett.* **2019**, *123*, No. 179601.
(134) Ritz, E. T.; Benedek, N. A. Ritz and Benedek Reply. *Phys. Rev. Lett.* **2019**, *123*, No. 179602.
(135) Dove, M. T. Flexibility of network materials and the Rigid Unit Mode model: a personal perspective. *Philos. Trans. R. Soc. A* **2019**, *377*, No. 20180222.

https://doi.org/10.1021/acs.jpcc.3c06507
J. Phys. Chem. C 2024, 128, 525−535